Trade-offs between effectiveness and cost in bifunctional enzyme circuit with concentration robustness

Shaohua Guan,[1,2] Liufang Xu,[3] Qing Zhang,[1] and Hualin Shi[1,2,*]

[1]*CAS Key Laboratory of Theoretical Physics, Institute of Theoretical Physics, Chinese Academy of Sciences, Beijing 100190, China*

[2]*School of Physical Sciences, University of Chinese Academy of Sciences, Beijing 100049, China*

[3]*Department of Physics and Biophysics & Complex System Center, Jilin University, Changchun 130012, Jilin, China*

(Received 10 May 2019; published 21 January 2020)

A fundamental trade-off in biological systems is whether they consume resources to perform biological functions or save resources. Bacteria need to reliably and rapidly respond to input signals by using limited cellular resources. However, excessive resource consumption will become a burden for bacteria growth. To investigate the relationship between functional effectiveness and resource cost, we study the ubiquitous bifunctional enzyme circuit, which is robust to fluctuations in protein concentration and responds quickly to signal changes. We show that trade-off relationships exist between functional effectiveness and protein cost. Expressing more proteins of the circuit increases concentration robustness and response speed but affects bacterial growth. In particular, our study reveals a general relationship between free-energy dissipation rate, response speed, and concentration robustness. The dissipation of free energy plays an important role in the concentration robustness and response speed. High robustness can only be achieved with a large amount of free-energy consumption and protein cost. In addition, the noise of the output increases with increasing protein cost, while the noise of the response time decreases with increasing protein cost. We also calculate the trade-off relationships in the EnvZ-OmpR system and the nitrogen assimilation system, which both have the bifunctional enzyme. Similar results indicate that these relationships are mainly derived from the specific feature of the bifunctional enzyme circuits and are not relevant to the details of the models. According to the trade-off relationships, bacteria take a compromise solution that reliably performs biological functions at a reasonable cost.

DOI: 10.1103/PhysRevE.101.012409

I. INTRODUCTION

Biochemical systems consist of a variety of biological molecules, including proteins, as well as various energy molecules, such as ATP and GTP. These systems need to reliably perform their biological functions, which is of great importance to the survival of the organism. The production of these biomolecules requires cellular materials as well as energy resources; in particular, the expression of proteins will occupy limited ribosomes. Overexpression of proteins will become a burden for cell growth. Previous experiments show that the expression of useless proteins decreases the growth rate of bacteria, which reduces the fitness of bacteria [1,2]. A cost function is introduced to characterize the extent of the use of cellular resources, which is an increasing function of protein expression levels [3]. Therefore, the reduction of biological fitness due to the consumption of resources, energy, and ribosomes in the protein expression can be represented by the protein expression levels. Reducing the protein cost or effectively performing functions is a fundamental trade-off in biological systems [4,5]. From the perspective of thermodynamics, biochemical systems are generally far away from the chemical equilibrium and require chemical free energy to perform functions. The trade-offs between biological functions and free-energy cost have been found in the proofreading mechanism [6], cellular computation [7], and regulatory system, including sensory [8–11] and oscillations [12–14]. However, the relationship between protein cost, free-energy cost, and functional effectiveness has not been fully investigated. In some biological systems, the relationship between the biological function and the amount of protein involved in the process is clear. For example, more ribosomes will provide more translational capacity during protein synthesis. However, in the sensing or signal regulatory systems, we do not know very well the effect of the different expression levels of the regulatory proteins, and the interplay between free-energy cost and protein expression levels is vague.

It is well known that sensing and regulatory systems need to accurately and rapidly sense environmental signals. However, fluctuations in molecular concentrations in the intracellular environment are inevitable. How these fluctuations affect information processing and how biological systems deal with such effects are important issues. It has been found that, in many sensing and regulatory systems, although the concentrations of the participating proteins fluctuate, the output signal at steady state does not change much. This kind of robustness, which is the insensitivity of the output signal to concentration fluctuations, is called concentration robustness [15,16]. A number of studies have been done on the robustness of bacterial chemotaxis [17–19] and other regulatory systems [20,21]. Concentration robustness of the two-component

*shihl@itp.ac.cn

system with bifunctional sensor kinase has also been studied theoretically and experimentally [22–24]. One of the most famous examples is the EnvZ-OmpR system, which is an osmotic-stress signaling system in bacteria. Many studies have investigated the relationship between concentration robustness and network structure of the EnvZ-OmpR system [25–27]. The bifunctional enzyme EnvZ has been found to be crucial for concentration robustness, and the specific structure has been identified in the biochemical reaction networks [15]. However, these studies focus on the structure of the network and ignore the impact of protein cost and free-energy cost.

Two types of functional effectiveness are considered in this article. The first one is how protein concentration fluctuations and internal noise of chemical reactions affect the fidelity of signal transduction. The second one is how fast the output signal responds to input signal changes. We consider two costs: protein cost and free-energy cost. The protein cost corresponds to the sum of all the various cellular resources required to express the proteins that make up the system, including energy and matter. It can be represented by the protein expression levels. The free-energy cost is the free energy consumed by the biological system in performing its function. We use a simple model with concentration robustness to investigate the relationship between biological functional effectiveness and costs. We found that both concentration robustness and response speed increase with increasing protein cost. This suggests that there is a trade-off between functional effectiveness and resource economy. We also revealed a general relationship between the free-energy dissipation rate, response speed, and concentration robustness. Only the system with high protein cost and free-energy cost can achieve high robustness. Moreover, the internal noise is also affected by the protein cost. The fluctuation of the output increases as the protein cost increases, but the fluctuation of the response time decreases as the protein cost increases. We also studied the EnvZ-OmpR system and the nitrogen assimilation system of *E. Coli* by numerical simulation. In these two different models, we got similar trade-off relationships, which implies that these trade-offs are based on the basic bifunctional feature of the circuit and are not affected by the network details. Furthermore, from the relationships between functional effectiveness and protein cost, we found that there is an appropriate region for protein cost in which relatively low protein cost could provide sufficiently high performance. This means that the system is both effective and economical in this region.

II. RESULTS

A. A simple model of the bifunctional enzyme circuit can provide concentration robustness

In this work, we focus on the biological circuit with a bifunctional enzyme. A key feature of this circuit is the bifunctional enzyme, which has a paradoxical effect. It activates and inhibits the regulatory protein [see Fig. 1(a)]. This particular feature is crucial for many biological functions, such as concentration robustness and ultrasensitivity in sensory systems, pattern formation, temporal pulses, and fold-change detection [24,27–30].

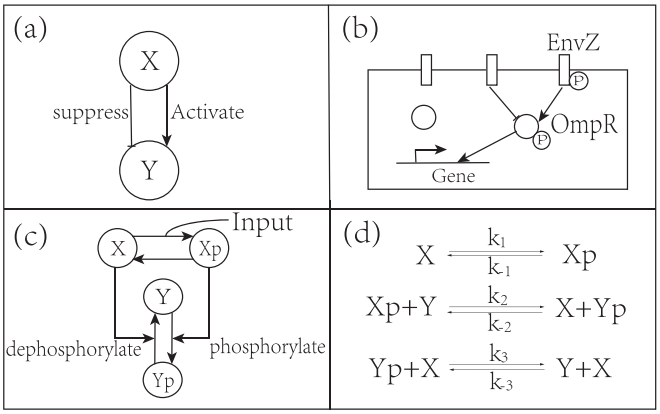

FIG. 1. The schematic diagram of the circuit with a bifunctional enzyme and its chemical reactions. (a) A schematic diagram of the system with a bifunctional enzyme. X activates protein Y and also inactivates Y. (b) A sketch map of the EnvZ-OmpR system of *E. coli*. EnvZ is a membrane-bound sensor kinase and bifunctional. The activated OmpR ($OmpR_p$) is regulated by EnvZ and regulates related gene expression. (c) This is a simple model of the circuit with a bifunctional enzyme. X is the bifunctional enzyme and Y is the regulator protein. X phosphorylates itself to X_p and then transfers the phosphoryl group to Y. The phosphorylated form of Y (Y_p) is dephosphorylated by X. The external input changes the rate of autophosphorylation of X. (d) Biochemical reactions of the simple model. The level of ATP, ADP, and Pi is assumed to be fixed. So k_1, k_{-1}, and k_{-3} include the concentration of ATP, ADP, and P_i, respectively ($k_1 = k_{10}$[ATP], $k_{-1} = k_{-10}$[ADP], and $k_{-3} = k_{-30}[P_i]$).

A well-studied system is the osmoregulation EnvZ-OmpR system of *E. Coli*. EnvZ is a membrane-bound sensor kinase. It can phosphorylate itself and then transfers the phosphoryl group to OmpR, an unphosphorylated response regulator. The bifunctional component EnvZ can dephosphorylate the phosphorylated OmpR [see Fig. 1(b)]. Here, we present a simple model based on the features of the EnvZ-OmpR system. In Fig. 1(c), the bifunctional enzyme and the regulator protein are denoted by X and Y, respectively. X phosphorylates itself to the phosphorylated form X_p and then transfers the phosphoryl group to Y. The phosphorylated form of Y represented by Y_p is dephosphorylated by X. We assume that these reactions are first-order reactions. The external input changes the autophosphorylation rate k_{10} of X, so we use this rate to represent the input signal. The phosphorylated form of Y (Y_p), which is the output of this simple model, regulates the expression of relevant genes. In addition, other molecules such as ATP, ADP, and P_i are also involved in the chemical reactions, and their concentrations affect the reaction rates. Instead of explicitly writing concentrations of these molecules, we combine them with the reaction rates to get effective reaction rates (k_1, k_{-1}, and k_{-3}) [see Fig. 1(d)]. The chemical kinetics of the simple model can be described by the following equations:

$$\frac{d[X]}{dt} = k_{-1}[X_p] + k_2[X_p][Y] - k_1[X] - k_{-2}[X][Y_p],$$

$$\frac{d[X_p]}{dt} = k_1[X] + k_{-2}[X][Y_p] - k_{-1}[X_p] - k_2[X_p][Y],$$

$$\frac{d[Y]}{dt} = k_{-2}[X][Y_p] + k_3[X][Y_p] - k_2[X_p][Y] - k_{-3}[X][Y],$$
$$\frac{d[Y_p]}{dt} = k_2[X_p][Y] + k_{-3}[X][Y] - k_{-2}[X][Y_p] - k_3[X][Y_p], \quad (1)$$

where $[X]$ and $[Y]$ are the concentrations of X and Y, and $[X_p]$ and $[Y_p]$ are the concentrations of X_p and Y_p. The total concentrations of X and Y satisfy $[X_t] = [X] + [X_p]$ and $[Y_t] = [Y] + [Y_p]$. In the chemical reactions, we introduce the reverse reactions of the signal transduction process because the free-energy dissipation of biochemical reactions is limited. Here, we use forward fluxes to represent the transduction process of the signal, and backward fluxes represent the reverse reactions of the transduction process. $k_{\pm i}$ denote the forward and backward reaction rates of the ith reaction.

It is known that biological systems need to dissipate energy to perform functions [6,8,12,31]. In the simple model, ATP is needed to drive the system away from equilibrium. We introduce γ to represent the reversibility of the signal transduction process, which is the ratio of forward fluxes to backward fluxes:

$$\gamma \equiv \frac{k_1 k_2 k_3}{k_{-1} k_{-2} k_{-3}} = \frac{k_{10} k_2 k_3 [\mathrm{ATP}]}{k_{-10} k_{-2} k_{-30} [\mathrm{ADP}][P_i]}.$$

When the system is in the equilibrium state, γ is equal to 1. When $\gamma > 1$, the forward fluxes are greater than the backward fluxes, which means that the system is transmitting signals from the input to the output and in a nonequilibrium state.

B. Trade-off between concentration robustness and protein cost

We first investigate how concentration robustness depends on protein cost. We assume that the time scale of this chemical reaction system is much smaller than that of expressing proteins X and Y. Therefore, we only consider the steady state of this system. Since the reverse reaction rates are smaller than the forward reaction rates in the simple model, the parameters in our model are restricted by $k_i \geqslant k_{-i}$. Under the physiological condition of *E. Coli,* the natural logarithm of γ is about $18k_BT$ ($\ln\gamma \approx 18k_BT$), which is equal to the chemical free energy released by hydrolysis of one ATP molecule [32]. For the sake of brevity, we set the thermal energy unit $k_BT = 1$. When the input signal is fixed, starting from the chemical kinetic equations (1), we derive the stable steady-state solution of the output, which is

$$[Y_p] = \frac{\alpha - \sqrt{\beta}}{2(k_2k_{-3} + k_2k_3)},$$

where α is $(k_2k_3 + 2k_2k_{-3})[Y_T] + (k_1k_2 + k_{-1}k_{-3} + k_{-1}k_{-2} + k_{-1}k_3)$, and β is $\alpha^2 - 4(k_2k_{-3} + k_2k_3)\{(k_1k_2 + k_{-1}k_{-3})[Y_T] + k_2k_{-3}[Y_T]^2\}$. For the sake of simplicity, we assume that reverse reaction rates k_{-1}, k_{-2}, and k_{-3} have the same value. Then $k_{-1}v = k_{-i} = \sqrt[3]{(k_1vk_2k_3)/\gamma}$ ($i = 2, 3$) and v is the unit of volume. Reaction rates (k_1, k_2, and k_3), protein cost ($[Y_t]$ and $[X_t]$), and γ determine the dynamics of the chemical kinetic equations (1). The steady-state solution of the output clearly shows that the output $[Y_p]$ is related to $[Y_t]$ without being affected by $[X_t]$. The relationship between $[Y_p]$ and $[Y_t]$ depends on γ. If $\gamma = 1$, which means the system is in chemical equilibrium, the output $[Y_p]$ is linear with $[Y_t]$. As γ becomes larger, the output $[Y_p]$ increases significantly as $[Y_t]$ increases when $[Y_t]$ is small, but it does not change much when $[Y_t]$ exceeds a certain value [see Fig. 2(a)]. If γ tends to infinity, reverse reaction rates k_{-i} ($i = 1, 2, 3$) will be 0. Then we get a simple solution:

$$[Y_p] = \begin{cases} [Y_t], & [Y_t] < k_1/k_3, \\ k_1/k_3, & [Y_t] \geqslant k_1/k_3, \end{cases}$$

which is derived in Appendix A. It shows that $[Y_t]$ has a threshold k_1/k_3. When $[Y_t]$ is less than the threshold, the output $[Y_p]$ will be equal to $[Y_t]$, and when $[Y_t]$ is greater than the threshold, the output $[Y_p]$ will be constant. When γ is a finite value, the change of $[Y_p]$ smoothly turns from the linear region to the constant region. The larger γ becomes, the smaller and the sharper the transition region will be. This threshold phenomenon also exists in other models, such as the receptor-ligand binding model and the Goldbeter-Koshland model [33]. In these models, the threshold phenomenon occurs only when parameters are at certain extreme conditions. For example, the affinity needs to be very high for the threshold phenomenon to occur in the receptor-ligand binding model. This extreme condition corresponds to the large γ in the simple model.

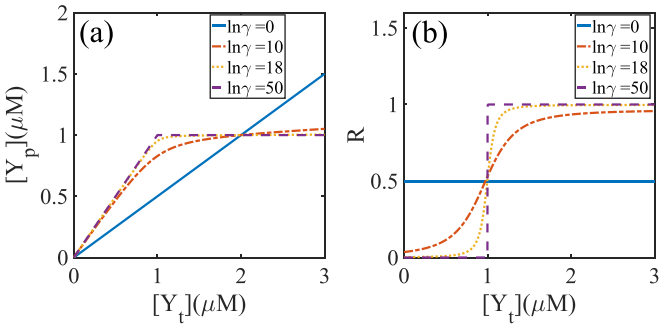

FIG. 2. The output $[Y_p]$ as a function of protein cost $[Y_t]$ and the relationship between robustness and $[Y_t]$ at different γ. (a) In the same external input, $[Y_p]$ increases with $[Y_t]$ linearly for small γ. When γ is large, $[Y_p]$ grows with $[Y_t]$ linearly and then reaches a plateau. (b) Robustness is a step function of $[Y_t]$ for large γ. The system will have high robustness at large $[Y_t]$. However, robustness is relatively low when γ is 0.

To quantify the concentration robustness of the simple model, we introduce

$$R([Y_t], \gamma) \equiv 1 - \frac{\partial [Y_p]([Y_t], \gamma)}{\partial [Y_t]}.$$

This quantity indicates the degree of change in output when the molecular concentration changes, which characterizes the robustness of the output to changes of molecular concentration $[Y_t]$. If the robustness is large, a change in $[Y_t]$ will result in a small change in the output $[Y_p]$. In contrast, small robustness implies that the output is sensitive to $[Y_t]$ variation. As shown in Fig. 2(b), the robustness is equal to 0.5 when the system is in chemical equilibrium ($\ln\gamma = 0$). However, if $\ln\gamma \gg 1$, the robustness jumps at the threshold $[Y_t] = k_1/k_3$. When $[Y_t]$ is less than the threshold, the output of the system is sensitive to changes of $[Y_t]$. If $[Y_t]$ is greater than the threshold, the output of the system is not sensitive to the change of

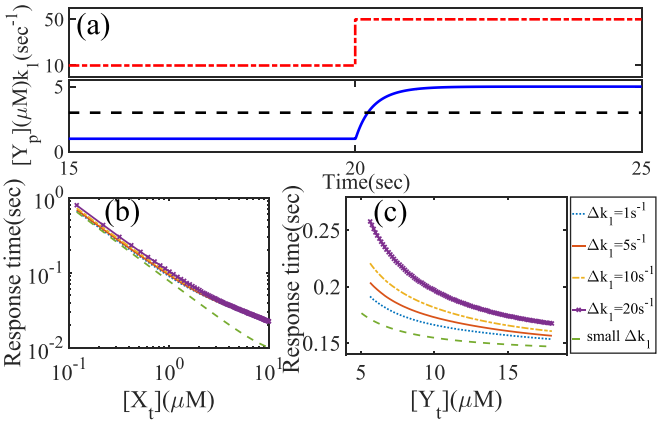

FIG. 3. A schematic diagram of the response time of the simple model and the relationship between response time and protein cost. (a) The input signal (dashed line) has a transition from 10 to 50 s^{-1} at time 20 s. Then output $[Y_p]$ shifts from a steady state to a poststimulus state. Response time is the time of output $[Y_p]$ from $[Y_{p0}]$ to $[Y_{p0}]+\frac{1}{2}[\Delta Y']$. (b) and (c) The relationship between response time and protein cost. Response time decreases with $[X_t]$, which has a slope of -1 in dual logarithm coordinate. Response time also decreases with $[Y_t]$. The dashed lines are the analytical results. Other lines are the simulation results solved by Runge-Kutta methods in different Δk_1.

$[Y_t]$, that is, the system is robust to the fluctuation of concentration $[Y_t]$. Under the physiological condition of biological systems ($\ln\gamma \approx 18$), robustness increases significantly with $[Y_t]$ and then raises slowly. The threshold phenomenon will be weakened when the system is in the physiological condition. The relationship between functional effectiveness and protein cost presents a trade-off phenomenon. Although a larger $[Y_t]$ leads to higher concentration robustness, resulting in higher fidelity of information processing, a higher protein expression level requires more cellular resources. The biological system faces a trade-off between concentration robustness and protein cost $[Y_t]$, which not only ensures the functional effectiveness but also makes the resource use economical. It can be seen from Fig. 2(b) that the system is effective and economical when $[Y_t]$ takes a value larger than the threshold but still close to the threshold. Compared with $[Y_t]$, the steady state of output $[Y_p]$ does not change with $[X_t]$. This means that the output of the system is always robust to $[X_t]$ variation. The absolute concentration robustness to $[X_t]$ variation is an intrinsic property of this simple model.

C. Trade-off between response time and protein cost

Another important function of sensing and regulatory systems is to respond quickly to changes in the input signal. A fast response can help the system quickly adjust its state. Therefore, we investigate the relationship between response speed and protein cost. When the input signal has a steplike variation, e.g., $k_1' = k_1 + \Delta k_1$, the output $[Y_p]$ will change from the previous steady state $[Y_{p0}]$ to the poststimulus steady state: $[Y_p'] = [Y_{p0}] + [\Delta Y']$ [see Fig. 3(a)]. We define the response time as the time of output $[Y_p]$ from $[Y_{p0}]$ to $[Y_{p0}]+\frac{1}{2}[\Delta Y']$. Linearization of the ordinary differential equations (1) near the previous steady state yields

$$\frac{d}{dt}[\Delta X] = -\{k_2([Y_t]-[Y_p]) + k_1 + k_{-2}[Y_p] + k_{-1}\}[\Delta X] - \{k_2([X_t]-[X]) + k_{-2}[X]\}[\Delta Y_p] - \Delta k_1[X],$$

$$\frac{d}{dt}[\Delta Y_p] = -\{k_2([Y_t]-[Y_p]) + (k_3+k_{-2})[Y_p] - k_{-3}([Y_t]-[Y_P])\}[\Delta X] - \{k_2([X_t]-[X]) + (k_{-2}+k_3)[X] + k_{-3}[X]\}[\Delta Y_p].$$

Due to the conservation of proteins, only two ordinary differential equations in (1) are independent. So we only need to write equations for $[\Delta X]$ and $[\Delta Y_p]$. For the sake of simplicity, after omitting the small reverse reactions and setting $k_2 = k_3$, the solution of these differential equations is

$$[\Delta Y_p] \approx \frac{\Delta k_1}{k_3}\left[1 - \exp\left(-\frac{k_3 t}{2}G\right)\right],$$

where $G = [X_t] + [Y_t] - \sqrt{[X_t]^2 + 2(2k_1/k_3 - [Y_t])[X_t] + [Y_t]^2}$. When $[\Delta Y_p]$ is equal to $\frac{1}{2}[\Delta Y']$, which is $\Delta k_1/(2k_3)$, $t = \frac{2\ln 2}{k_3}G^{-1}$. As shown in Fig. 3(b), the simulation results show that the logarithm of response time has a negative linear correlation with the logarithm of $[X_t]$. This result can be obtained from the analytical result with a reasonable approximation. Under the condition of $[X_t] \ll [Y_t]$, G can be approximated as $2[X_t]$. Then

$$t = \frac{\ln 2}{k_3}[X_t]^{-1}. \tag{2}$$

The slope of the function between $[X_t]$ and t in double logarithmic coordinates is -1, which is consistent with the slope of the simulation results. Under the nonextreme condition $[X_t] < [Y_t]$, the response time will also be affected by $[Y_t]$. As shown in Fig. 3(c), the response time also decreases with $[Y_t]$. However, the scale of response time that varied with $[Y_t]$ is much smaller than the scale that varied with $[X_t]$. This indicates that the response time is mainly affected by $[X_t]$. The analytical results are located below the simulated results. The reason is that the response time increases with Δk_1 and our analytical results are approximate results when Δk_1 is very small.

Figures 3(b) and 3(c) show that the response time decreases with $[X_t]$ and $[Y_t]$. It suggests that there is a trade-off between response time and protein cost. The more protein the cell expresses, the shorter the response time of this system will be. In actual biological systems, such as the EnvZ-OmpR system and the nitrogen assimilation system, the concentration of bifunctional enzyme ($[X_t]$) is far less than the concentration of another protein ($[Y_t]$) [22,34]. This means that the approximately linear relationship between $[X_t]$ and t in double logarithmic coordinates is present in actual biological systems. The more interesting phenomenon is that $[X_t]$ is the main factor affecting the response time under the constraint of the actual biological system ($[X_t] \ll [Y_t]$). $[Y_t]$ is the main factor affecting concentration robustness. $[X_t]$ and $[Y_t]$ play different roles in regulating the system functions. This suggests that the biological system can adjust the concentration robustness and response speed by regulating $[X_t]$ and $[Y_t]$, respectively. This may be a design principle, i.e., the biological system evolves

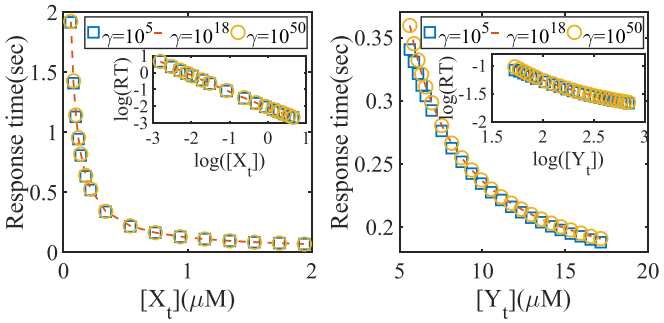

FIG. 4. Relationship between response time and protein cost at different γ. When γ changes from 10^5 to 10^{50}, there is no obvious change in the relationships between response time and protein cost ($[X_t]$ or $[Y_t]$). These curves are almost overlapping.

into controlling functions by regulating the concentration of the functionally coupled protein and removing the coupling between functions and other proteins.

The parameter γ plays an important role in concentration robustness. Does the γ also have a large impact on the response time? We change γ by adjusting the reverse reaction rates, and we calculate how the response time varies with the protein concentrations $[X_t]$ and $[Y_t]$. As shown in Fig. 4, these relations do not have significant changes. This indicates that the variation of γ does not influence the response time.

D. Energy-speed-robustness trade-off relation for bifunctional enzyme circuits with concentration robustness

Free-energy dissipation is important for many biological processes. We can compute the free-energy dissipation rate:

$$\dot{W} = \sum_i (J_i^+ - J_i^-) \ln \frac{J_i^+}{J_i^-},$$

where J_i^+ and J_i^- are the rates of ith forward and backward reaction fluxes [35,36]. In our model, the free-energy dissipation rate at steady state is expressed as

$$\dot{W} = [X_t]\xi(k_3[Y_p] - k_{-3}[Y])\ln\gamma,$$

where $\xi = [X]/[X_t]$. The steady-state values of ξ, $[Y_p]$, and $[Y]$ are determined by $[Y_t]$ and γ. The free-energy dissipation rate is linear with $[X_t]$ at fixed Y_t and γ, which means the system dissipates more free energy at higher $[X_t]$. However, the relationship between the free-energy dissipation rate and $[Y_t]$ changes with γ. As shown in Fig. 5(a), when $\ln\gamma$ is small,

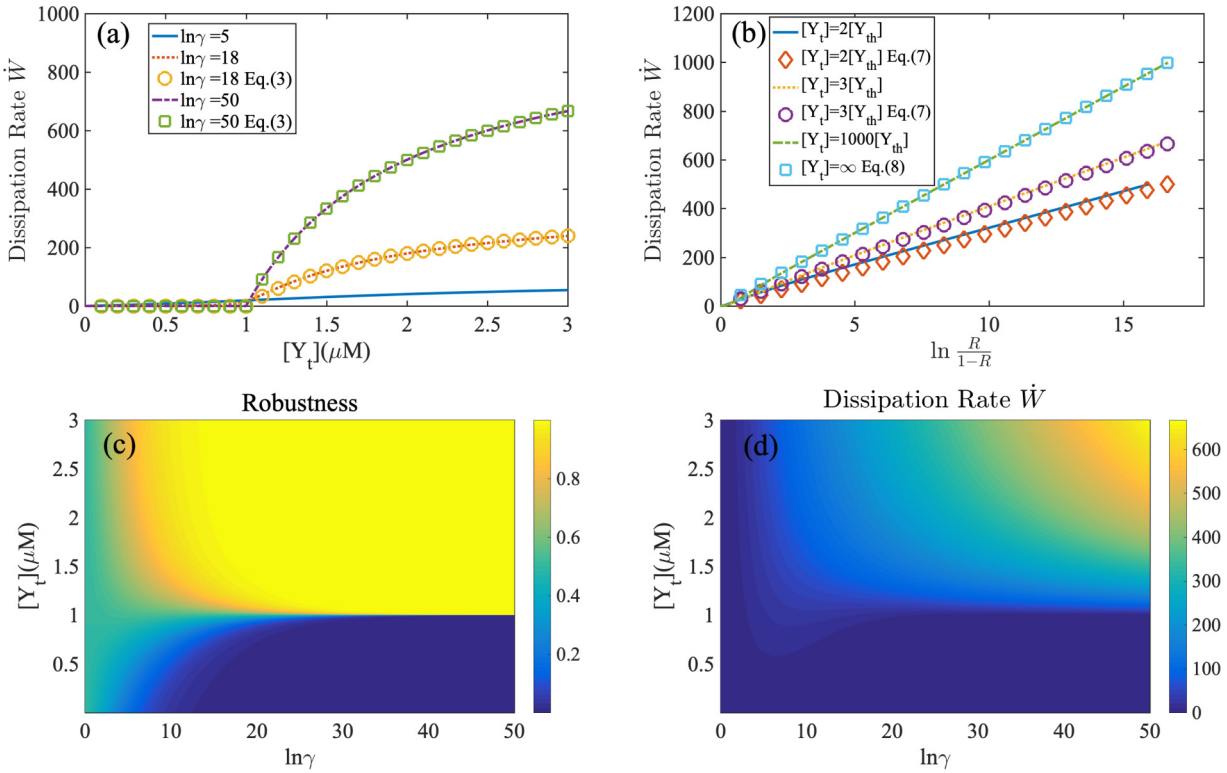

FIG. 5. The relationship between the free-energy dissipation rate and concentration robustness. (a) The relationship between the free-energy dissipation rate $\dot{W}$ and $[Y_t]$ changes with γ. When γ is small, $\dot{W}$ increases with $[Y_t]$ slowly. But for large γ, $\dot{W}$ is near 0 when $[Y_t] < k_1/k_3$ and then gradually increases with $[Y_t]$. The squares and circles are the solutions of Eq. (3). (b) The relationship between the free-energy dissipation rate $\dot{W}$ and robustness at different $[Y_t]$. Lines are simulation results and others are analytical results. As $[Y_t]$ and R becomes larger, the simulation and analytical results are more consistent. (c) and (d) Contour plots of the free-energy dissipation rate and robustness in $(\ln\gamma, [Y_t])$ space. The system has low robustness and a small free-energy dissipation rate if γ or $[Y_t]$ is low. At the high level of γ and $[Y_t]$, robustness is close to 1 and $\dot{W}$ is very large. Enough protein $[Y_t]$ and free-energy dissipation rate are necessary for the system to be robust. At large γ, the system has two states that have high robustness and low robustness. $[Y_{th}] = k_1/k_3 = 1\ \mu$M is the boundary of these two states.

the dissipation rate gradually grows with $[Y_t]$. As $\ln\gamma$ increases, a threshold equal to the transition point k_1/k_3 appears. Below the threshold, the system almost does not dissipate energy. When $[Y_t]$ exceeds the threshold, the dissipation rate increases with $[Y_t]$. Under the assumption of $k_i \gg k_{-i}$, the terms with k_{-i} in $\xi(k_3[Y_p] - k_{-3}[Y])$ could be omitted, and the free-energy dissipation rate can be approximated as (see details in Appendix B)

$$\dot{W} = \begin{cases} 0, & [Y_t] < [Y_{\rm th}], \\ k_1[X_t]\ln\gamma\,\frac{[Y_t]-k_1/k_3}{k_1/k_2+([Y_t]-k_1/k_3)}, & [Y_t] \geqslant [Y_{\rm th}], \end{cases} \tag{3}$$

where $[Y_{\rm th}]$ is the threshold value k_1/k_3 at infinitely large γ. If the parameter $k_2 = k_3$, Eq. (3) has a simpler form:

$$\dot{W} = \begin{cases} 0, & [Y_t] < [Y_{\rm th}], \\ k_1[X_t]\ln\gamma\,\frac{([Y_t]-[Y_{\rm th}])}{[Y_t]}, & [Y_t] \geqslant [Y_{\rm th}]. \end{cases} \tag{4}$$

When $[Y_t] \gg [Y_{\rm th}]$, we can approximately write $\dot{W} = k_1[X_t]\ln\gamma$. This indicates that $\dot{W}$ increases with γ logarithmically in the region of high $[Y_t]$. γ varies in different physiological conditions because of different energy-bearing biomolecules, such as ATP, GTP, and SAM, or variations of their concentrations. The logarithmic dependence of the free-energy dissipation rate on γ suggests that an energy-bearing molecule with large energy (e.g., ATP) or high concentration leads to a large free-energy dissipation rate.

Concentration robustness and response time are closely related to the free-energy dissipation rate because they are all related to protein cost or γ. When $[Y_t]$ is larger than the threshold, concentration robustness increases with γ and approaches a constant as $[Y_t]$ becomes larger and larger. When $[Y_t]$ is large enough, concentration robustness can be approximated as (see details in Appendix C)

$$R = \frac{k_3}{k_3 + \sqrt[3]{(k_1 v k_2 k_3)/\gamma}}, \tag{5}$$

which means concentration robustness is only related to reaction rates and γ. Moreover, as shown in Eq. (2), response time is determined by $[X_t]$ and k_3. Response time and the free-energy dissipation rate are related by $[X_t]$ rather than γ, while concentration robustness and the free-energy dissipation rate are related through γ. Combined with Eqs. (2), (3), and (5), we can get the energy-speed-robustness relation (see details in Appendix C)

$$\dot{W} = \ln 2\,\frac{[Y_{\rm th}]([Y_t]-k_1/k_3)}{k_1/k_2+([Y_t]-k_1/k_3)}\omega\left[\ln\phi + 3\ln\left(\frac{R}{1-R}\right)\right], \tag{6}$$

where ω is the response speed t^{-1} and ϕ is $k_1 v k_2/k_3^2$. If we assume $k_2 = k_3$, the relation will be

$$\dot{W} = \ln 2\,\frac{[Y_{\rm th}]([Y_t]-[Y_{\rm th}])}{[Y_t]}\omega\left[\ln([Y_{\rm th}]v) + 3\ln\left(\frac{R}{1-R}\right)\right], \tag{7}$$

where $[Y_{\rm th}]$ represents the threshold value k_1/k_3, and v is the unit of volume. When $[Y_t] \gg [Y_{\rm th}]$,

$$\dot{W} = \ln 2[Y_{\rm th}]\omega\left[\ln([Y_{\rm th}]v) + 3\ln\left(\frac{R}{1-R}\right)\right]. \tag{8}$$

The above equations are good approximations when $[Y_t]$ and γ are relatively large. When $[Y_t]$ is larger than the threshold value, concentration robustness increases with γ from 0.5 to 1 [see Fig. 2(b)]. Then $\ln(R/1-R)$ also increases with γ from 0 to infinity. As shown in Fig. 5(b), the analytical results of Eqs. (7) and (8) are in good agreement with the numerical simulation results at large $[Y_t]$ and γ, where curves have a large slope and R. The simple energy-speed-robustness relation clearly shows that more functional effectiveness needs a larger free-energy dissipation rate. This is a fundamental trade-off relation in circuits with concentration robustness. It is also interesting to note that the energy-speed-robustness relation is similar to the energy-speed-accuracy trade-off relation in sensory adaptation [8].

The energy-speed-robustness trade-off relation is valid at large $[Y_t]$ and γ. We further investigate the relationship between robustness and energy dissipation rate in the condition of small $[Y_t]$ and γ. In parameter space $(\ln\gamma, [Y_t])$, these two quantities are strongly correlated [see Figs. 5(c) and 5(d)]. In the upper right corner of the parameter space, high concentration robustness is accompanied by a large free-energy dissipation rate. Moreover, they have an identical threshold, i.e., $[Y_{\rm th}] = k_1/k_3$, at a relatively large $\ln\gamma$. This boundary separates the robust and sensitive regimes, which correspond to the dissipative and nondissipative states, respectively. Both large $\ln\gamma$ and $[Y_t]$ are necessary conditions for the system to maintain a dissipative and robust state. Robustness is enhanced with a large free-energy dissipation rate in the robust regime $[Y_t] > k_1/k_3$. This is qualitatively consistent with Eq. (6) and the energy-accuracy trade-off in the proofreading process and sensory adaptation system [6,8].

E. Protein cost affects noise of output and response time

The process of gene expression is stochastic [37]. The fluctuation of protein expression levels may affect biological system functions. In Sec. II B, we studied how the average of the output varies with protein levels. However, the fidelity of signal transduction is also inevitably reduced by the internal noise of chemical reactions, which may depend on the amount of protein in the signal transduction system. Here, we further investigate how the amount of protein affects the internal noise in the simple model. The previous study has discussed how free-energy dissipation affects function and noise [38]. And a stochastic study has been used to compare the differences between monofunctional and bifunctional two-component systems and study the relationship between system output noise and external stimulus [39]. In this section, we use the chemical master equation to investigate how protein cost affects the output noise and the response time noise.

The chemical master equation of the simple model is shown in Appendix D. When the noise is relatively small, the linear noise approximation is useful to study the stochastic behavior at steady state [40]. The master equation can be approximated as a linear Fokker-Planck equation, and the stationary distribution is a multivariate Gaussian distribution. The covariance matrix of variable fluctuations $\boldsymbol{C}$ is determined by the Lyapunov matrix equation $\boldsymbol{AC} + \boldsymbol{CA}^T + \boldsymbol{D} = \boldsymbol{0}$. $\boldsymbol{A}$ is the Jacobian matrix and $\boldsymbol{D}$ is the diffusion matrix ($\boldsymbol{D} \equiv \boldsymbol{BB}^T$). The variance of output N_{Y_p} is shown in Appendix D. The Fano factor is viewed as a kind of noise-to-signal ratio, which is defined as $F_x = \sigma_x^2/\mu_x$ for variable x. σ_x^2 and μ_x are the

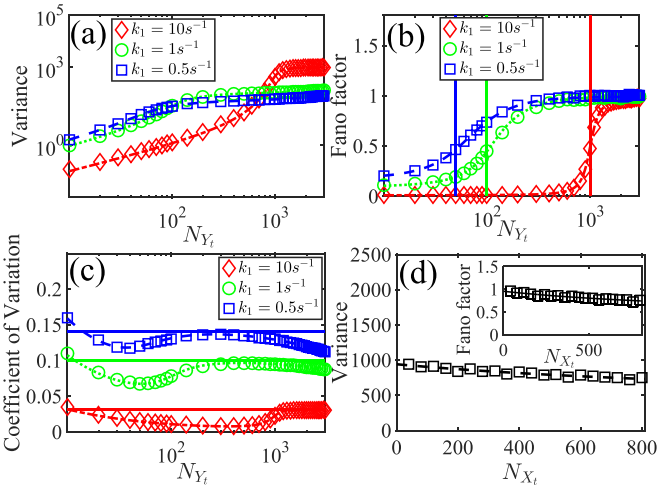

FIG. 6. Relationships between the noise of output and protein costs. (a) and (b) Variance and Fano factor of output increase with N_{Y_t} and reach a peak at large N_{Y_t}. The solid lines represent the threshold at different k_1. (c) The coefficient of variation changes with N_{Y_t}. They are close to the value of $1/\sqrt{N_{Y_{\text{th}}}}$ of each input k_1 (solid lines). $N_{Y_{\text{th}}}$ is the protein number of N_{Y_p} at the threshold. (d) More N_{X_t} will slightly reduce variance and the Fano factor of output. In (a), (b), and (c), the number of N_{X_t} is 100. In (d), the number of N_{Y_t} is 1500. The unit of abscissa is the protein number. The dashed lines are obtained from the linear noise approximation, and others are the Gillespie algorithm results.

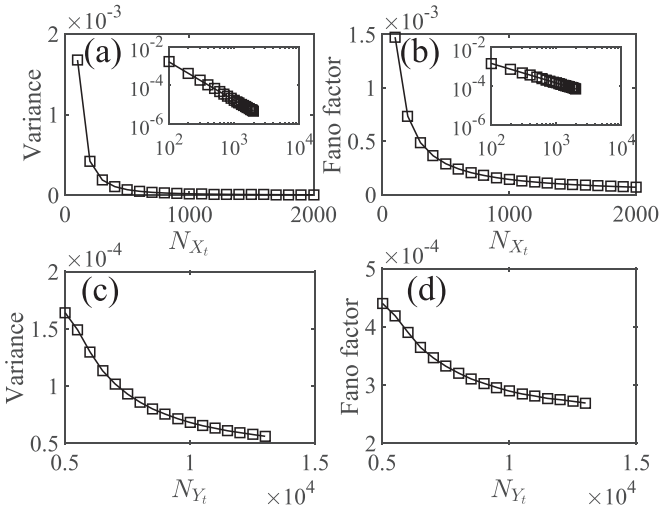

FIG. 7. Relationship between response time noise and protein cost. The logarithm of variance and Fano factor of response time has a linear relation with the logarithm of N_{X_t}. This is similar to the relation between the average response time and $[X_t]$. In (a) and (b), the number of N_{Y_t} is 10 000. In (c) and (d), the number of N_{X_t} is 500. The unit of abscissa is the protein number.

variance and mean value of random variable x, respectively. The stochastic behavior of output could be described by the variance and Fano factor.

We also simulated the simple model by the Gillespie algorithm and got the distribution of output N_{Y_p} at steady state. The Gillespie algorithm is a well-known stochastic simulation algorithm (SSA) to generate the stochastic trajectory of the signal transduction process (see details in Sec. IV B) [41]. Moreover, the response time could be calculated as the first passage time by setting a threshold in output N_{Y_p} [42].

As shown in Figs. 6(a) and 6(b), the output variance and Fano factor are relatively low when protein number N_{Y_t} is low. When N_{Y_t} gradually exceeds the threshold $N_{Y_{\text{th}}}$ ($N_{Y_{\text{th}}} = k_1 V/k_3$), the variance and Fano factor increase with N_{Y_t} and reach a plateau. The output N_{Y_p} and threshold are affected by the input k_1. We further investigate how the variance and Fano factor change with input k_1. The variance decreases with input k_1 at the low level of N_{Y_t} and increases with input k_1 at the high level of N_{Y_t}. But the Fano factor always decreases with input k_1. Moreover, as the input k_1 increases, the Fano factor curve becomes steeper and steeper. When protein number N_{Y_t} is large, the Fano factor under different input signals approaches 1, which is the Fano factor of the Poisson process. It is consistent with the results of [43,44], which show that the quasistationary distribution of the output approaches a Poisson distribution in the case of large numbers of molecules. When the protein number N_{Y_t} is small, the system output exhibits sub-Fano behavior. This is because the steady-state value of the output N_{Y_p} is very close to N_{Y_t} [see Fig. 2(a) and Appendix A]. The output fluctuates around the steady-state value and the fluctuation is approximately the order of magnitude of the distance between steady-state value N_{Y_p} and N_{Y_t}. Therefore, sub-Fano behavior will appear when N_{Y_t} is small. It must be noted that the fluctuations of N_{Y_t} itself are not considered here. Below the threshold, the fluctuation of N_{Y_t} has a great influence on the fluctuation of the output, while above the threshold the fluctuation of N_{Y_t} has a small effect on the fluctuation of the output. This also shows that the average value and fluctuation of the output are both robust to concentration fluctuations at large N_{Y_t}. To compare the relative variability of the output at different input k_1, the coefficient of variation is used. As shown in Fig. 6(c), the coefficient of variation of output N_{Y_p} decreases with input signal k_1. It fluctuates with the increase of N_{Y_t} but is always smaller than $1/\sqrt{N_{Y_{\text{th}}}}$ unless N_{Y_t} is very small. It suggests that the relative variability of the output is large when the input signal is small. Compared with N_{Y_t}, the output noise does not change significantly with N_{X_t} [see Fig. 6(d)].

The relationship between the average response time and protein cost has been shown in Sec. II C. In Fig. 7, the variance and Fano factor of the response time also have a negative linear relationship with N_{X_t} in dual logarithm coordinate, which is similar to the relationship between the average response time and $[X_t]$. This result implies that expressing more protein X will reduce the noise of the response time. It is consistent with the result in [45], which suggests that the variance of response time decreases with the number of receptors. N_{Y_t} does not have a linear relationship with the variance and the Fano factor of the response time. However, the magnitudes of variance and the Fano factor vary little with N_{Y_t}. It suggests N_{Y_t} does not have an obvious effect on the noise of the response time.

In conclusion, protein cost has a large impact on the output and response time, affecting not only their average value but also their noise. Consistent with the previous results regarding different roles of proteins in functions, protein cost N_{Y_t} mainly

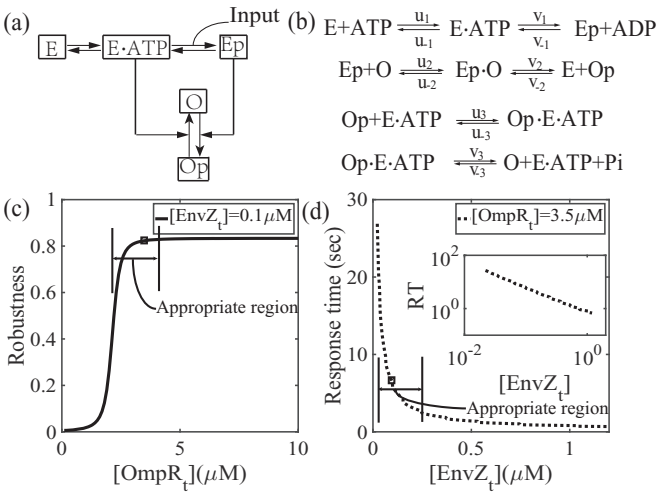

FIG. 8. A sketch map of the modified Shinar model of the EnvZ-OmpR system and relationships between functional effectiveness and protein cost. (a) and (b) The modified Shinar model [24] of the EnvZ-OmpR system. E and O represent EnvZ and OmpR, respectively. $E \cdot \mathrm{ATP}$ is the enzyme that dephosphorylates O_p. (c) and (d) The relationship between robustness and $[\mathrm{OmpR}_t]$ (response time and $[\mathrm{EnvZ}_t]$) is similar to Fig. 2(b) [Fig. 3(b)]. The appropriate region represents high functional effectiveness and relatively low protein cost. Black squares are the protein expression levels in *E. Coli* [22].

affects the variance and Fano factor of the output, and N_{X_t} mainly affects the variance and Fano factor of the response time. More N_{X_t} will reduce the variance of the response time, while more N_{Y_t} will increase the variance of the output, and the Fano factor approaches 1 at large N_{Y_t}.

F. EnvZ-OmpR system and nitrogen assimilation system have similar trade-offs

The circuits with a bifunctional enzyme have been found in many biological systems. It carries out crucial functions in sensing environmental signals and regulating metabolism signals [24,28–30]. Are our results based on the simple model still valid in these biological systems with the similar feature? Do the details of the system affect the behavior of the system? We choose the EnvZ-OmpR system and the nitrogen assimilation system to discuss these issues. The EnvZ-OmpR system and the nitrogen assimilation system have similar bifunctional enzyme circuits, and both have concentration robustness [24,29]. We want to know if these systems have similar relationships between functions and protein cost.

1. The modified Shinar model of the EnvZ-OmpR system

The Shinar model of the EnvZ-OmpR system has more complex biochemical details than our simple model [24]. EnvZ and OmpR can combine with other molecules, such as ATP, so this model involves many intermediate protein complexes. The phosphorylated OmpR is dephosphorylated by EnvZ-ATP, which is crucial to cause absolute concentration robustness [15] [see Figs. 8(a) and 8(b)]. Here, we included small reverse reactions in this model to investigate the relationship between functions and protein cost. Because of the small reverse reactions, the modified Shinar model does not have absolute concentration robustness. The concentration robustness is determined by the molecular concentration and free-energy cost. By numerically solving the biochemical reaction kinetic equations described in Fig. 8(b), we obtain the relationships between functions and protein costs, as shown in Figs. 8(c) and 8(d), which are very similar to what we obtained in the simple model. It indicates that these relationships are not influenced by the details of the model. It can be seen from Fig. 8(c) that as the OmpR concentration increases, the concentration robustness of the system increases, but when the OmpR concentration exceeds a certain value, the benefit of adding OmpR is no longer obvious. Figure 8(d) shows that as the concentration of EnvZ increases, the response speed of the system becomes faster, and similarly when EnvZ exceeds a certain value, the increase of response speed is no longer obvious with the increase of EnvZ. Since the expression of these proteins requires cellular resources, achieving sufficient biological functional effectiveness at the least possible protein cost has an evolutionary advantage. From Figs. 8(c) and 8(d), it is obvious that the system is both economical and effective in the appropriate region, that is, the system can obtain high functional effectiveness while the protein cost is relatively low. From [22], we know that the concentrations of EnvZ and OmpR are about 0.1 and 3.5 μM, respectively. Using black squares to display these values in Figs. 8(c) and 8(d), we find that they fall in the appropriate region. This seems to indicate that the expression levels of EnvZ and OmpR are optimized in evolution based on the trade-off between function and cost. If the protein cost is lower than the appropriate region, the biological system will lose a lot of concentration robustness and response speed. If the cost of protein exceeds these regions too much, it will waste a lot of protein and bring little benefit to the system.

2. Nitrogen assimilation system

We want to know if similar relationships exist in other regulatory systems with a bifunctional enzyme. We consider the nitrogen assimilation system, which can regulate the ratio of glutamine and α-ketoglutarate robustly. In the nitrogen assimilation system, glutamine synthetase (GS) converts glutamate and ammonia to glutamine. GS has two states: GS modified with the adenyl and unmodified GS. Adenylyltransferase (AT/AR) is the bifunctional enzyme, which adenylates or deadenylates glutamine synthetase [see Figs. 9(a) and 9(b)]. Thus, the two states of glutamine synthetase can be converted into each other under the catalysis of the same enzyme. To avoid waste, even if the concentrations of enzyme GS and AT/AR fluctuate, a fixed ratio should be maintained between the substrate (α-ketoglutarate) and product (glutamine). This concentration robustness makes the ratio of glutamine and α-ketoglutarate insensitive to the fluctuations of the AT/AR and GS concentrations. We use a simple model from [29] to examine the effects of fluctuations of GS and AT/AR on system concentration robustness and response speed. By numerically solving the biochemical reaction kinetic equation described in Fig. 9(b), we obtained the relationship between robustness and GS concentration [see Fig. 9(c)] and the relationship between response time and AT/AR concentration [see

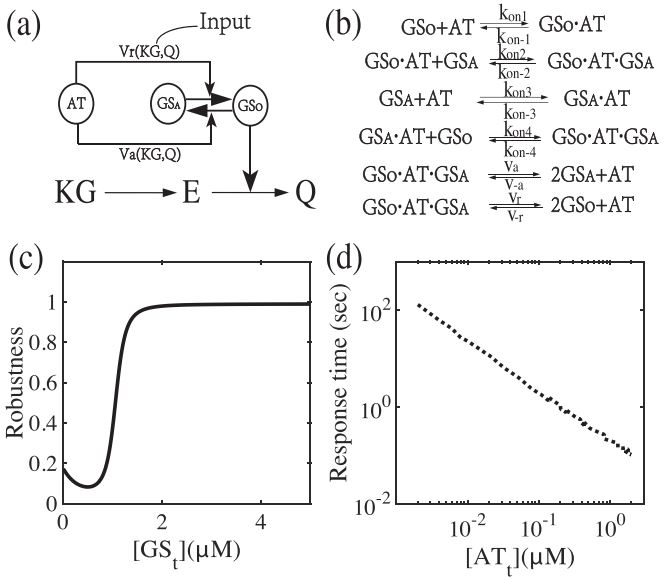

FIG. 9. A sketch map of the nitrogen assimilation system and relationships between functional effectiveness and protein cost. (a) and (b) AT/AR (abbreviated as AT) is the bifunctional enzyme. Reaction parameters V_a and V_r are regulated by α-ketoglutarate (KG) and glutamine (Q). The output is the steady-state level of GS_o, which regulates the ratio of the substrate (KG) to the product (Q). (c) and (d) When $[GS_t]$ is small, the robustness-$[GS_t]$ relation in the nitrogen assimilation system is a little different from the relation in the EnvZ-OmpR system. But at large $[GS_t]$, the relationship between robustness and $[GS_t]$ is similar to Fig. 2(b). The speed-$[AT_t]$ relation is also linear in the dual logarithm coordinates.

Fig. 9(d)], which are similar to the relationships in the simple model. In double logarithmic coordinates, the response time also has a negative linear relationship with the AT/AR concentration. It suggests that these trade-offs between functional effectiveness and protein cost are based on the feature of the circuit with bifunctional enzyme and do not depend on specific parameters and details of the network.

III. DISCUSSION

Previous research has focused on the relationship between function and free-energy cost. For example, the proofreading process, which was first proposed by Hopfield [46], has a trade-off between free-energy cost and accuracy [6]. Lan *et al.* [8] found an energy-speed-accuracy trade-off in the sensory adaptation system. Both studies have shown that energy cost can improve the performance of the biological system. In this work, we also reveal a general relation between energy dissipation rate, response speed, and concentration robustness. Both high robustness and fast response speed need a high-energy dissipation rate. In addition, we also consider another kind of cost, namely the protein cost. Evolutionary experiments have demonstrated that the level of protein is optimized [3]. Therefore, cells need to use protein resources economically and effectively to achieve the desired biological functions, especially in the case of limited cellular resources. Our results revealed the general relationship between functional effectiveness (concentration robustness and responding speed) and protein cost in the circuits with a bifunctional enzyme. Our results showed that concentration robustness is independent of the bifunctional protein cost, which is an intrinsic property of the bifunctional circuits. When the system is far from equilibrium, the relationship between concentration robustness and regulatory protein cost has two different regimes: a sensitive regime and a robust regime. Enough regulatory protein cost is needed for the system to be robust. However, the response time is mainly affected by the bifunctional protein cost and decreases as the level of bifunctional protein increases. Different protein costs control the different parts of the system performance, not only the concentration robustness and response speed but also the variances of output and response speed. This feature, in which the concentration robustness and response speed are controlled by different protein costs, helps the biological system achieve its desired functional effectiveness by separately adjusting the corresponding protein expression levels. For example, if the system needs faster response speed, it only needs to increase the expression of the bifunctional protein, while the robustness does not change. This may be a design principle behind the evolution of the bifunctional circuits.

These relationships between functional effectiveness and protein cost lead to an interesting question. What is the appropriate expression level of the relevant protein to perform a function? Comparing with free-energy cost, molecular concentration is easily regulated. Changes in ATP concentration will affect other functions of the cell. However, regulation of the relevant molecular concentration will only affect the performance of that function. In the small timescale, molecular concentration could be regulated to a desirable level by a regulatory factor. From an evolutionary standpoint, the molecular expression level will be changed with DNA sequences of gene regulatory regions in a few hundred generations [3]. It is easy to evolve the protein level to an appropriate region. From the functional effectiveness and protein cost relationships, we can get another important piece of information. The system will get more performance at a higher protein cost, but when the performance is near optimal, further increases in protein cost will bring less benefit to biological system performance [47]. It is uneconomical to increase the protein cost for a small increase in performance. Moreover, a low protein expression level leads to a large loss of functional effectiveness. So we proposed that there is an economic and effective protein cost region between these two extreme conditions.

An important result of our article is that trade-off relations of our simple model based on bifunctional circuits are universal. Although different biological systems, such as the EnvZ-OmpR system and the nitrogen assimilation system, have similar circuits with a bifunctional enzyme, the biochemical reactions of these two systems have different details. Interestingly, the trade-off relationship calculated from these two systems, which have different parameters and network structures, are consistent with the results of the simple model. This suggests that the trade-off relationship between functional effectiveness and protein cost is universal. It may depend on the basic bifunctional feature of the circuit. Finding the general relationship between functional effectiveness and protein cost in more biological systems would be an interesting topic.

Interestingly, the energy-speed-accuracy relation in sensory adaptation [8] has a similar form with our energy-speed-robustness relation in circuits with concentration robustness. The adaptation speed and the response speed in these two systems are linear with the free-energy dissipation rate. Furthermore, both adaptation error and concentration robustness have the natural logarithm relation with the free-energy dissipation rate. It is interesting to find more relationships between energy and performance in other systems. There may be a universal relationship between a specific function, speed, and energy dissipation rate in many biological systems.

IV. METHODS

A. Numerical simulation parameters

In the simple model, the steady-state level of output $[Y_p]$ is obtained by integrated the differential equations (1) in the fourth-order Runge-Kutta method. The forward reaction rate k_1 is 10 s^{-1} if k_1 is not explicitly stated. k_2 and k_3 are 10 $\mu M^{-1} s^{-1}$. Reverse reaction rates k_{-1}, k_{-2}, and k_{-3} are set to the same value and estimated from γ. $k_{-1}v = k_{-i} = \sqrt[3]{(k_1 v k_2 k_3)/\gamma}$ $(i = 2, 3)$ and v is the unit of volume. Parameters in the Shinar model of the EnvZ-OmpR system are the same as in [24], which are [ATP] = 1000 μM [48], $P_i = 1000$ μM, [ADP] = 50 μM [49], $u_1 = u_2 = u_3 = 100$ $\mu M^{-1} s^{-1}$, $u_{-1} = 6000$ s^{-1} [50], $u_{-2} = 200$ s^{-1} [51], $u_{-3} = 200$ s^{-1}, $v_1 = v_2 = v_3 = 10$ s^{-1}, $v_{-1} = v_{-2} = 0.01$ $\mu M^{-1} s^{-1}$, and $v_{-3} = 0.01$ $\mu M^{-2} s^{-1}$. The reverse reaction rates v_{-1}, v_{-2}, and v_{-3} are obtained from $\gamma \approx 10^9$. Parameters of the nitrogen assimilation system model are $k_{on1} = k_{on2} = k_{on3} = k_{on4} = 100$ $\mu M^{-1} s^{-1}$, $k_{on-1} = k_{on-2} = k_{on-3} = k_{on-4} = 50$ s^{-1}, $V_a = V_r = 3$ s^{-1}, and $V_{-a} = V_{-r} = 0.1$ $\mu M^{-2} s^{-1}$. Concentration of KG is 1 μM.

B. Stochastic simulation method

To get variances of output and response time, we use the Monte Carlo (Gillespie algorithm [41]) simulation. The Gillespie algorithm, developed by Daniel T. Gillespie in the 1970s, is well known as an effective stochastic simulation algorithm. The reaction probability density function $P(\tau, \mu)$ is calculated, where τ is the time when the next chemical reaction occurs and μ represents which chemical reaction occurs. Then the molecular number of relevant species will be renewed. In this way, we obtain statistically correct trajectories of the chemical system time evolution. It is also effective for calculating the Fano factor and response time. We use the mean first passage time (MFPT) to describe the response time of the system [42,52]. It theoretically represents the time it takes, on average, to reach a boundary the first time. This threshold value is the average of the mean value of output before and after input change in the steady state. Finally, we obtain the MFPT by averaging the results, which is repeatedly calculated 200 000 times. All simulation parameters were presented in Sec. IV A, and γ is 10^6.

ACKNOWLEDGMENTS

The work was supported by the Strategic Priority Program of Chinese Academy of Sciences (Grant No. XDA17010504), National Natural Science Foundation of China (Grants No. 11774359 and No. 11947302), and the Interdisciplinary Innovation Team of Chinese Academy of Sciences (Grant No. 2060299).

APPENDIX A: DERIVATION OF THE STEADY STATE OF $[Y_p]$ AT INFINITELY LARGE γ

The stable steady-state solution of the output is expressed as

$$[Y_p] = \frac{\alpha - \sqrt{\beta}}{2(k_2 k_{-3} + k_2 k_3)},$$

where α is $(k_2k_3 + 2k_2k_{-3})[Y_T] + (k_1k_2 + k_{-1}k_{-3} + k_{-1}k_{-2} + k_{-1}k_3)$ and β is $\alpha^2 - 4(k_2k_{-3} + k_2k_3)\{(k_1k_2 + k_{-1}k_{-3})[Y_T] + k_2k_{-3}[Y_T]^2\}$. When γ is infinite, the reverse reaction rates k_{-i} $(i = 1, 2, 3)$ turn out to be 0. Ignoring items with reverse reaction rates in α and β, α becomes $k_2k_3[Y_t] + k_1k_2$ and $\sqrt{\beta}$ is $|k_2k_3[Y_t] - k_1k_2|$. If $[Y_t] \geqslant k_1/k_3$, $\sqrt{\beta}$ becomes $k_2k_3[Y_t] - k_1k_2$, and if $[Y_t]$ is less than k_1/k_3, $\sqrt{\beta}$ is $k_1k_2 - k_2k_3[Y_t]$. Therefore, k_1/k_3 is a threshold for $[Y_t]$. At the infinite large γ,

$$[Y_p] = \begin{cases} [Y_t], & [Y_t] < k_1/k_3, \\ k_1/k_3, & [Y_t] \geqslant k_1/k_3. \end{cases}$$

In the condition of large γ and small $[Y_t]$, the steady-state output can be approximated as

$$[Y_p] \approx [Y_t] - \frac{k_{-1}k_3}{k_2(k_3 + k_{-3})} \frac{[Y_t]}{k_1/k_3 - [Y_t]}.$$

The last term is small when reverse reaction rates and $[Y_t]$ are small.

APPENDIX B: DERIVATION OF EQ. (3)

The free-energy dissipation rate is $\sum_i (J_i^+ - J_i^-) \ln \frac{J_i^+}{J_i^-}$. In the simple model, there are three pairs of fluxes: $J_1^+ - J_1^- = k_1[X] - k_{-1}[X_p]$, $J_2^+ - J_2^- = k_2[X_p][Y] - k_{-2}[X][Y_p]$, and $J_3^+ - J_3^- = k_3[X][Y_p] - k_{-3}[X][Y]$. At the steady state, these three pairs of fluxes are equal. Therefore, the free-energy dissipation rate of the simple model at the steady state is $\dot{W} = (J_3^+ - J_3^-) \ln \gamma = (k_3\xi[X_t][Y_p] - k_{-3}\xi[X_t][Y]) \ln \gamma$, where $\xi = [X]/[X_t]$. The steady-state solution ξ of chemical kinetic equations (1) is

$$\xi = \frac{k_{-1} + k_2[Y_t] - k_2[Y_p]}{k_{-1} + k_1 + k_{-2}[Y_p] + k_2([Y_t] - [Y_p])}.$$

Under the approximation of $k_i \gg k_{-i}$ $(i = 1, 2, 3)$, terms in $k_3\xi[Y_p] - k_{-3}\xi[Y]$ with reverse reaction rates could be omitted, which is

$$k_3\xi[Y_p] - k_{-3}\xi[Y] = k_3 \frac{k_2([Y_t] - [Y_p])}{k_1 + k_2([Y_t] - [Y_p])}[Y_p].$$

As shown in Appendix A, $[Y_p]$ can be approximated as a piecewise function under the condition of small reverse reaction rates. Therefore, the free-energy dissipation rate is

$$\dot{W} = \begin{cases} 0, & [Y_t] < k_1/k_3, \\ [X_t] \ln \gamma \frac{k_1k_2([Y_t] - k_1/k_3)}{k_1 + k_2([Y_t] - k_1/k_3)}, & [Y_t] \geqslant k_1/k_3. \end{cases}$$

If we assume $k_2 = k_3$, it will be

$$\dot{W} = \begin{cases} 0, & [Y_t] < [Y_{\text{th}}], \\ k_1[X_t] \ln\gamma \frac{([Y_t]-[Y_{\text{th}}])}{[Y_t]}, & [Y_t] \geqslant [Y_{\text{th}}], \end{cases}$$

where $[Y_{\text{th}}]$ is the threshold value k_1/k_3 at infinitely large γ.

APPENDIX C: DERIVATION OF THE ENERGY-SPEED-ROBUSTNESS RELATION

The concentration robustness is

$$R([Y_t], \gamma) \equiv 1 - \frac{\partial[Y_p]([Y_t], \gamma)}{\partial[Y_t]} = \frac{k_2k_3 + \frac{\beta'}{2\sqrt{\beta}}}{2(k_2k_{-3} + k_2k_3)}$$

and

$$\beta'/\sqrt{\beta} = \frac{2k_2^2k_3^2[Y_t] + \theta}{\sqrt{k_2^2k_3^2[Y_t]^2 + \theta[Y_t] + \rho}},$$

where θ is $2(-k_1k_2^2k_3 + k_2k_3^2k_{-1} + k_2k_3k_{-1}k_{-3} + k_2k_3k_{-1}k_{-2} + 2k_2k_{-1}k_{-2}k_{-3})$ and ρ is $(k_1k_2 + k_3k_{-1} + k_{-1}k_{-3} + k_{-1}k_{-2})^2$. If $[Y_t]$ is large, $\beta'/\sqrt{\beta}$ can be approximated as $2k_2k_3$. Then the concentration robustness is $k_3/(k_3 + k_{-3})$ at large $[Y_t]$. Because the reverse reaction rate $k_{-3} = \sqrt[3]{k_1vk_2k_3/\gamma}$, R is $k_3/(k_3 + \sqrt[3]{k_1vk_2k_3/\gamma})$ and $\ln\gamma$ will be $\ln\phi + 3\ln[R/(1-R)]$, where ϕ is k_1vk_2/k_3^2. Moreover, if we assume $k_2 = k_3$, ϕ will become $[Y_{\text{th}}]v$.

From Eq. (2), protein cost $[X_t]$ is $\omega \ln 2/k_3$. ω is the response speed t^{-1}. Then we can get the energy-speed-robustness relation

$$\dot{W} = \ln 2 \frac{[Y_{\text{th}}]([Y_t] - k_1/k_3)}{k_1/k_2 + ([Y_t] - k_1/k_3)} \omega \left[\ln\phi + 3\ln\left(\frac{R}{1-R}\right)\right].$$

To obtain the above relation, the protein cost $[Y_t]$ and γ should be relatively large.

APPENDIX D: CHEMICAL MASTER EQUATION AND LINEAR NOISE APPROXIMATION FOR THE SIMPLE MODEL

Biochemical reactions of the simple model can be described by the chemical master equation, which is

$$\begin{aligned}
\frac{dP(N_{Y_p}, N_X)}{dt} &= k_1(N_X+1)P(N_{Y_p}, N_X+1) - k_1N_XP(N_{Y_p}, N_X) \\
&+ k_2\frac{(N_{Y_t} - N_{Y_p} + 1)(N_{X_t} - N_X + 1)}{V}P(N_{Y_p} - 1, N_X - 1) - k_2\frac{(N_{Y_t} - N_{Y_p})(N_{X_t} - N_X)}{V}P(N_{Y_p}, N_X) \\
&+ k_3\frac{(N_{Y_p}+1)N_X}{V}P(N_{Y_p}+1, N_X) - k_3\frac{N_{Y_p}N_X}{V}P(N_{Y_p}, N_X) \\
&+ k_{-1}(N_{X_t} - N_X + 1)P(N_{Y_p}, N_X - 1) - k_{-1}(N_{X_t} - N_X)P(N_{Y_p}, N_X) \\
&+ k_{-2}\frac{(N_{Y_p}+1)(N_X+1)}{V}P(N_{Y_p}+1, N_X+1) - k_{-2}\frac{N_{Y_p}N_X}{V}P(N_{Y_p}, N_X) \\
&+ k_{-3}\frac{(N_{Y_t} - N_{Y_p} + 1)N_X}{V}P(N_{Y_p} - 1, N_X) - k_{-3}\frac{(N_{Y_t} - N_{Y_p})N_X}{V}P(N_{Y_p}, N_X).
\end{aligned}$$

N represents the number of protein and V is the system volume. From the master equation, we can get the Jacobian matrix

$$\boldsymbol{A} = \begin{bmatrix} -k_1 - k_{-1} - k_2\overline{[Y]} - k_{-2}\overline{[Y_p]}, & -k_2\overline{[X_p]} - k_{-2}\overline{[X]} \\ (k_{-3} - k_2)\overline{[Y]} - (k_{-2} + k_3)\overline{[Y_p]}, & -k_2\overline{[X_p]} - (k_{-2} + k_3 + k_{-3})\overline{[X]} \end{bmatrix}$$

and the diffusion matrix

$$\boldsymbol{D} = \begin{bmatrix} J_1^+ + J_1^- + J_2^+ + J_2^-, & J_2^+ + J_2^- \\ J_2^+ + J_2^-, & J_2^+ + J_2^- + J_3^+ + J_3^- \end{bmatrix},$$

where J_i^+ and J_i^- are the rates of ith forward and backward reaction fluxes. The rates of reaction fluxes are

$$\begin{aligned}
J_1^+ &= k_1\overline{[X]}, \quad J_1^- = k_{-1}\overline{[X_p]}, \\
J_2^+ &= k_2\overline{[X_p]}\,\overline{[Y]}, \quad J_2^- = k_{-2}\overline{[X]}\,\overline{[Y_p]}, \\
J_3^+ &= k_3\overline{[X]}\,\overline{[Y_p]}, \quad J_3^- = k_{-3}\overline{[X]}\,\overline{[Y]}.
\end{aligned}$$

The concentration of molecule with a bar represents the steady-state value of its concentration.

From the Lyapunov matrix equation $\boldsymbol{AC} + \boldsymbol{CA}^T + \boldsymbol{D} = \boldsymbol{0}$, we can get the variance of output concentration $[Y_p]$:

$$\boldsymbol{C}_{22} = \frac{\boldsymbol{A}_{21}^2\boldsymbol{D}_{11} - (\boldsymbol{A}_{12}\boldsymbol{A}_{21} - \boldsymbol{A}_{11}^2 - \boldsymbol{A}_{11}\boldsymbol{A}_{22})\boldsymbol{D}_{22} - 2\boldsymbol{A}_{11}\boldsymbol{A}_{21}\boldsymbol{D}_{12}}{2\boldsymbol{A}_{22}(\boldsymbol{A}_{12}\boldsymbol{A}_{21} - \boldsymbol{A}_{11}^2 - \boldsymbol{A}_{11}\boldsymbol{A}_{22}) + 2\boldsymbol{A}_{11}\boldsymbol{A}_{12}\boldsymbol{A}_{21}}.$$

Then the variance of output N_{Y_p} is $\boldsymbol{C}_{22}V$. V is the volume of an *E. Coli* cell, which is about $V = 10^{-15}$ L [22]. The molecular concentration 1 μM corresponds to the molecular number $n_aV \times 10^{-6} \approx 600$, where n_a is Avogadro's number. For numerical simplicity, we set 1 μM corresponding to the molecular number 1000. Then, the volume is about 1.67×10^{-15} L.

[1] M. Scott, C. W. Gunderson, E. M. Mateescu, Z. Zhang, and T. Hwa, Science **330**, 1099 (2010).
[2] Q. Zhang, R. Li, J. Li, and H. Shi, Biophys. J. **115**, 896 (2018).
[3] E. Dekel and U. Alon, Nature (London) **436**, 588 (2005).
[4] P. Szekely, H. Sheftel, A. Mayo, and U. Alon, PLoS Comput. Biol. **9**, e1003163 (2013).
[5] J. Hausser, A. Mayo, L. Keren, and U. Alon, Nat. Commun. **10**, 68 (2019).
[6] A. Murugan, D. A. Huse, and S. Leibler, Proc. Natl. Acad. Sci. (USA) **109**, 12034 (2012).
[7] P. Mehta and D. J. Schwab, Proc. Natl. Acad. Sci. (USA) **109**, 17978 (2012).
[8] G. Lan, P. Sartori, S. Neumann, V. Sourjik, and Y. Tu, Nat. Phys. **8**, 422 (2012).
[9] G. Lan and Y. Tu, J. R. Soc., Interface **10**, 20130489 (2013).
[10] P. Sartori, L. Granger, C. F. Lee, and J. M. Horowitz, PLoS Comput. Biol. **10**, e1003974 (2014).
[11] C. C. Govern and P. R. ten Wolde, Phys. Rev. Lett. **113**, 258102 (2014).
[12] Y. Cao, H. Wang, Q. Ouyang, and Y. Tu, Nat. Phys. **11**, 772 (2015).
[13] C. Fei, Y. Cao, Q. Ouyang, and Y. Tu, Nat. Commun. **9**, 1434 (2018).
[14] A. C. Barato and U. Seifert, Phys. Rev. X **6**, 041053 (2016).
[15] G. Shinar and M. Feinberg, Science **327**, 1389 (2010).
[16] J. M. Eloundou-Mbebi, A. Küken, N. Omranian, S. Kleessen, J. Neigenfind, G. Basler, and Z. Nikoloski, Nat. Commun. **7**, 13255 (2016).
[17] U. Alon, M. G. Surette, N. Barkai, and S. Leibler, Nature (London) **397**, 168 (1999).
[18] N. Barkai and S. Leibler, Nature (London) **387**, 913 (1997).
[19] T.-M. Yi, Y. Huang, M. I. Simon, and J. Doyle, Proc. Natl. Acad. Sci. (USA) **97**, 4649 (2000).
[20] N. Barkai and B.-Z. Shilo, Mol. Cell **28**, 755 (2007).
[21] R. Silva-Rocha and V. de Lorenzo, Annu. Rev. Microbiol. **64**, 257 (2010).
[22] S. J. Cai and M. Inouye, J. Biol. Chem. **277**, 24155 (2002).
[23] E. Batchelor and M. Goulian, Proc. Natl. Acad. Sci. (USA) **100**, 691 (2003).
[24] G. Shinar, R. Milo, M. R. Martínez, and U. Alon, Proc. Natl. Acad. Sci. (USA) **104**, 19931 (2007).
[25] O. A. Igoshin, R. Alves, and M. A. Savageau, Mol. Microbiol. **68**, 1196 (2008).
[26] M. Goulian, Curr. Opin. Microbiol. **13**, 184 (2010).
[27] R. Straube, PLoS Comput. Biol. **10**, e1003614 (2014).
[28] G. Shinar, J. D. Rabinowitz, and U. Alon, PLoS Comput. Biol. **5**, e1000297 (2009).
[29] Y. Hart, D. Madar, J. Yuan, A. Bren, A. E. Mayo, J. D. Rabinowitz, and U. Alon, Mol. Cell **41**, 117 (2011).
[30] Y. Hart and U. Alon, Mol. Cell **49**, 213 (2013).
[31] L. Xiong and G. Lan, PLoS Comput. Biol. **11**, e1004351 (2015).
[32] D. L. Nelson, A. L. Lehninger, and M. M. Cox, *Lehninger Principles of Biochemistry* (Macmillan, New York, 2008).
[33] R. Straube, Biosystems **162**, 215 (2017).
[34] G.-W. Li, D. Burkhardt, C. Gross, and J. S. Weissman, Cell **157**, 624 (2014).
[35] H. Qian, Annu. Rev. Phys. Chem. **58**, 113 (2007).
[36] H. Ge and H. Qian, Phys. Rev. E **81**, 051133 (2010).
[37] J. M. Raser and E. K. O'shea, Science **309**, 2010 (2005).
[38] P. Sartori and Y. Tu, Phys. Rev. Lett. **115**, 118102 (2015).
[39] A. K. Maity, A. Bandyopadhyay, P. Chaudhury, and S. K. Banik, Phys. Rev. E **89**, 032713 (2014).
[40] J. Elf and M. Ehrenberg, Genome Res. **13**, 2475 (2003).
[41] D. T. Gillespie, J. Phys. Chem. **81**, 2340 (1977).
[42] Y. Hao, L. Xu, and H. Shi, J. Mol. Biol. **406**, 195 (2011).
[43] D. F. Anderson, G. A. Enciso, and M. D. Johnston, J. R. Soc., Interface **11**, 20130943 (2014).
[44] D. F. Anderson, D. Cappelletti, and T. G. Kurtz, SIAM J. Appl. Dyn. Syst. **16**, 1309 (2017).
[45] X. Cheng, L. Merchan, M. Tchernookov, and I. Nemenman, Phys. Biol. **10**, 035008 (2013).
[46] J. J. Hopfield, Proc. Natl. Acad. Sci. (USA) **71**, 4135 (1974).
[47] N. Tokuriki, C. J. Jackson, L. Afriat-Jurnou, K. T. Wyganowski, R. Tang, and D. S. Tawfik, Nat. Commun. **3**, 1257 (2012).
[48] D. A. Schneider and R. L. Gourse, J. Biol. Chem. **279**, 8262 (2004).
[49] P. R. Jensen and O. Michelsen, J. Bacteriol. **174**, 7635 (1992).
[50] L. Plesniak, Y. Horiuchi, D. Sem, D. Meinenger, L. Stiles, J. Shaffer, P. A. Jennings, and J. A. Adams, Biochemistry **41**, 13876 (2002).
[51] K. Mattison and L. J. Kenney, J. Biol. Chem. **277**, 11143 (2002).
[52] Y. Lan and G. A. Papoian, Phys. Rev. Lett. **98**, 228301 (2007).